Optimization of dual-core and microstructure fiber geometries for dispersion compensation and large mode area

A. Huttunen
Department of Electrical and Communications Engineering, Laboratory of Computational Engineering, Helsinki University of Technology, FIN-02015 HUT, Finland
anu.huttunen@hut.fi

P. Törmä
Department of Physics, Nanoscience Center, FIN-40014 University of Jyväskylä, Finland

Abstract: We investigate dual concentric core and microstructure fiber geometries for dispersion compensation. Dispersion values as large as -59 000 ps/(nm km) are achieved, over a broad wavelength range with full width at half maximum exceeding 100 nm. The trade-off between large dispersion and mode area is studied. Geometries with an effective mode area of $30\mu m^2$ and dispersion -19 000 ps/(nm km) and $80\mu m^2$ with -1600 ps/(nm km) are proposed.

OCIS codes: (060.2310) Fiber optics; (060.2340) Fiber optics components; (060.2400) Fiber properties.

References and links

1. T. A. Birks, D. Mogilevtsev, J. C. Knight, and P. St.J. Russel, "Dispersion compensation using single-material fibers," IEEE Photon. Tech. Lett. **11,** 674–676 (1999).
2. L. P. Shen, W.-P. Huang, G. X. Chen, and S. S. Jian, "Design and optimization of photonic crystal fibers for broad-band dispersion compensation," IEEE Photon. Tech. Lett. **15,** 540–542 (2003).
3. L. P. Shen, W.-P. Huang, and S. S. Jian, "Design of photonic crystal fibers for dispersion-related applications," J. Lightwave Tech. **21,** 1644–1651 (2003).
4. R. K. Sinha and S. K. Varshney, "Dispersion properties of photonic crystal fibers," Microwave and Optical Tech. Lett. **37,** 129–132 (2003).
5. F. Poli, A. Cucinotta, M. Fuochi, S. Selleri, and L. Vincetti, "Characterization of microstructured optical fibers for wideband dispersion compensation," J. Opt. Soc. Am. A **20,** 1958–1962 (2003).
6. Y. Ni, L. An, J. Peng, and C. Fan, "Dual-core photonic crystal fiber for dispersion compensation," IEEE Photon. Tech. Lett. **16,** 1516–1518 (2004).
7. B. Zsigri, J. Laegsgaard, and A. Bjarklev, "A novel photonic crystal fibre design for dispersion compensation," J. Opt. A: Pure Appl. Opt. **6,** 717–720 (2004).
8. K. Thyagarajan, R. K. Varshney, P. Palai, A. K. Ghatak, and I. C. Goyal, "A novel design of a dispersion compensating fiber," IEEE Photon. Technol. Lett. **8,** 1510–1512 (1996).
9. J.-L. Auguste, R. Jindal, J.-M. Blondy, M. Clapeau, J. Marcou, B. Dussardier, G. Monnom, D. B. Ostrowsky, B. P. Pal, and K. Thyagarajan, "-1800 ps(nm.km) chromatic dispersion at $1.55\mu m$ in dual cocentric core fibre," Electronics Lett. **36,** 1689–1691 (2000).
10. L. Grüner-Nielsen, S. N. Knudsen, B. Edvold, T. Veng, D. Magnussen, C. C. Larsen, and H. Damsgaard, "Dispersion compensating fibers," Opt. Fiber Technol. **6,** 164–180 (2000).
11. J. L. Auguste, J. M. Blondy, J. Maury, J. Marcou, B. Dussardier, G. Monnom, R. Jindal, K. Thyagarajan, and B. P. Pal, "Conception, realization, and characterization of a very high negative chromatic dispersion fiber," Opt. Fiber Technol. **8,** 89–105 (2002).

#5959 - $15.00 US Received 2 December 2004; revised 13 December 2004; accepted 18 January 2005

12. K. Pande and B. P. Pal, "Design optimization of a dual-core dipersion-compensating fiber with a high figure of merit and a large effective area for dense wavelength-division multiplexed transmission through standard G.655 fibers," Appl. Opt. **42,** 3785–3791 (2003).
13. M. Ibanescu, Y. Fink, S. Fan, E. L. Thomas, and J. D. Joannopoulos, "An all-dielectric coaxial waveguide," Science **289,** 415 (2000).
14. G. Ouyang, Y. Xu, and A. Yariv, "Theoretical study on dispersion compensation in air-core Bragg fibers," Opt. Express **10,** 899–908 (2002), http://www.opticsexpress.org/abstract.cfm?URI=OPEX-10-17-899.
15. T. D. Engeness, M. Ibanescu, S. G. Johnson, O. Weisberg, M. Skorobogatiy, S. Jacobs, and Y. Fink, "Dispersion tailoring and compensation by model interactions in OmniGuide fibers," Opt. Express **11,** 1175–1196 (2003), http://www.opticsexpress.org/abstract.cfm?URI=OPEX-11-10-1175.
16. C. D. Poole, J. M. Wiesenfeld, D. J. DiGiovanni, and A. M. Vengsarkar, "Optical fiber-based dispersion compensation using higher order modes near cutoff", J. Lightwave Technol. **12,** 1746–1758 (1994).
17. A. H. Gnauck, L. D. Garrett, Y. Danziger, U. Levy, and M. Tur, "Dispersion and dispersion-slope compensation of NZDSF over the entire C band using higher-order-mode fibre," Electronics Lett. **36,** 1946–1947 (2000).
18. S. Ramachandran, B. Mikkelsen, L. C. Cowsar, M. F. Yan, G. Raybon, L. Boivin, M. Fishteyn, W. A. Reed, P. Wisk, D. Brownlow, R. G. Huff, and L. Gruner-Nielsen, "All-fiber grating-based higher order mode dispersion compensator for broad-band compensation and 1000-km transmission at 40 Gb/s," IEEE Photon. Tech. Lett. **13,** 632–634 (2001).
19. S. Ghalmi, S. Ramachandran, E. Monberg, Z. Wang, M. Yan, F. Dimarello, W. Reed, P. Wisk, and J. Fleming, "Low-loss, all-fibre higher-order-mode dispersion compensators for lumped or multi-span compensation," Electronics Lett. **38,** 1507–1508 (2002).
20. S. G. Johnson and J. D. Joannopoulos, "Block-iterative frequency-domain methods for Maxwell's equations in a planewave basis," Opt. Express **8,** 173–190 (2001), http://www.opticsexpress.org/abstract.cfm?URI=OPEX-8-3-173.
21. G. P. Agrawal, *Nonlinear Fiber Optics* (Academic, London, 1995).
22. R. Iliew, C. Etrich, and F. Lederer, "Remote coupling in Bragg fibers," Opt. Lett. **29,** 1596–1598 (2004).
23. M. Vaziri and C.-L. Chen, "An etched two-mode fiber modal coupling element," J. Lightwave Tech. **15,** 474–480 (1997).

1. Introduction

The fibers that have been installed for long-haul data transmission were designed for wavelengths around 1300 nm. Thus they have large dispersion values for wavelengths around 1500 nm, employed after the development of Erbium-doped fiber amplifier. The magnitude of the dispersion parameter for such a standard single mode fiber is of the order of $D = 10 \ldots 20$ ps/(nm km). Dispersion causes pulses to spread and has to be compensated for in the long distance optical data transmission systems. One way to realize this is to use dispersion compensating fibers, which are designed to have large negative dispersion. The commercial dispersion compensation fibers usually have dispersion values of $D = -100$ to -300 ps/(nm km). In order to minimize losses, the dispersion compensating fibers should be as short as possible and thus the magnitude of negative dispersion should be as large as possible.

Photonic crystal fibers or microstructure fibers can be designed to have large absolute values of the dispersion parameter and thus they have potential for dispersion compensation applications [1, 2, 3, 4, 5, 6, 7]. In photonic crystal fibers dispersion values up until -18000 ps/(nm km) [6] have been predicted by numerical considerations. Another type of fiber having a large dispersion is dual-core fiber [8, 9, 10, 11, 12]. For dual-core fiber dispersion of -1800 ps/(nm km) has been experimentally shown [9] and -5100 ps/(nm km) predicted [8]. Third type of fiber exhibiting large dispersion is Bragg-fiber [13, 14, 15]. Extremely large dispersion values of over -500000 ps/(nm km) were predicted [15]. Fourth type of dispersion compensating fiber is a multimode fiber, whose higher order mode exhibits high dispersion [16, 17, 18, 19]. The dispersion values of the higher-order-mode fibers are generally less than -1000 ps/(nm km).

Here we study microstructure fiber geometries that have a high index core and a defect ring of reduced hole diameter in the cladding and similar dual-core fiber geometries. The largest dispersion values we predict are $D = -55000$ ps/(nm km) for microstructure fiber and $D = -59000$ ps/(nm km) for dual-core fiber, which are both considerably larger than the previously

#5959 - $15.00 US Received 2 December 2004; revised 13 December 2004; accepted 18 January 2005

considered values for these types of fibers.

Large dispersion is usually found in fibers with small mode areas. This limits the power that can be put through the fiber since nonlinear effects become too severe. Secondly, the mode area of a dispersion compensating fiber should be as close as possible to the mode area of a standard optical fiber in order to reduce splice loss. Currently, mode field diameters of dispersion compensation fibers are usually around 5 μm [10], whereas the mode field diameters of standard optical fiber are around 10 μm. The mode areas of photonic crystal fibers with high dispersion are very small, usually around 1 $\mu\mathrm{m}^2$. The largest predicted mode area for dispersion compensating photonic crystal fiber is 12 $\mu\mathrm{m}^2$ [6]. Mode areas of Bragg fibers are comparable to the standard optical fiber [15], but the splice loss is high because of the interface between the air and silica cores of Bragg- and standard optical fiber, respectively. The mode areas of the higher-order-mode fibers are of the order of $70\mu\mathrm{m}^2$ [17], comparable to those of standard optical fiber.

We have investigated the trade-off between large mode area and dispersion. We achieved mode area of 30 $\mu\mathrm{m}^2$ with dispersion $D = -19000$ ps/(nm km) for both the microstructure fiber and the dual-core fiber. Mode area 80 $\mu\mathrm{m}^2$ comparable to that of the standard optical fiber has dispersion -1600 ps/(nm km). This type of large mode area dispersion compensating fiber can be used for dispersion compensation of high power pulses or for simultaneous amplification and dispersion compensation by doping the fiber with, for example, Erbium.

Another issue to be considered is the wavelength range of high dispersion. The bands of the Erbium doped fiber amplifier used in the dense wavelength division multiplexing (DWDM) networks are the C band (1530–1565 nm) and the L band (1570–1610 nm). Thus the full with at half maximum of the negative dispersion should span around 100 nm wide spectrum in order to efficiently compensate the dispersion of all the frequencies of the DWDM systems. There is also a trade-off between large dispersion and wide FWHM of the dispersion compensating fibers. The FWHM of the dual core fiber with $D = -1800$ ps/(nm km) is only 20 nm [9] and the dispersion of a broad band design is less than -200 ps/(nm km) [11]. The Bragg fiber with $D = -500000$ ps/(nm km) has a FWHM of approximately 20 nm [15]. The photonic crystal fiber design with $D = -18000$ has FWHM of only around 4 nm [6]. The band widths of the higher-order-mode fibers are greater than 40 nm [18]. All the geometries investigated in this paper have FWHM wider than 100 nm.

2. Geometries of the microstructure and dual-core fibers

The material of the studied microstructure fibers is taken to be silica (refractive index $n = 1.444$). The cladding is formed by a triangular lattice of air holes. The radius of the air holes is $r = 0.38P$, where P is the period of the cladding lattice. The core radius is $r_{core} = 0.5P$ and the refractive index of the core n_{core} is varied between $1.5 \ldots 2.8$. One ring of the air holes is made to form a defect ring in the otherwise periodic cladding (see Fig. 1). Three geometries with a different type of a defect ring are studied. They are shown in Fig. 1(a)-(c).

The geometry of the dual-core fiber is illustrated in Fig. 1(d). The cladding of the dual-core fiber has a refractive index 1.2114, which is the average index of the microstructure fiber cladding. The studied inner core indeces are the same than for the microstructure fibers. The outer core index is taken to represent the three microstructure geometries in Fig. 1(a)-(c), and is taken to have corresponding average indices 1.444, 1.3859, and 1.299. Radius of the inner core is $r_{core} = 0.5P$. The outer core covers the region $r = 2.5 \ldots 3.5P$.

3. Numerical method

The dispersion of the fibers is calculated with a full-vectorial plane wave method (the MIT Photonic bands software) [20]. First, the effective index n_{eff} of the fiber is calculated as a function

#5959 - $15.00 US Received 2 December 2004; revised 13 December 2004; accepted 18 January 2005

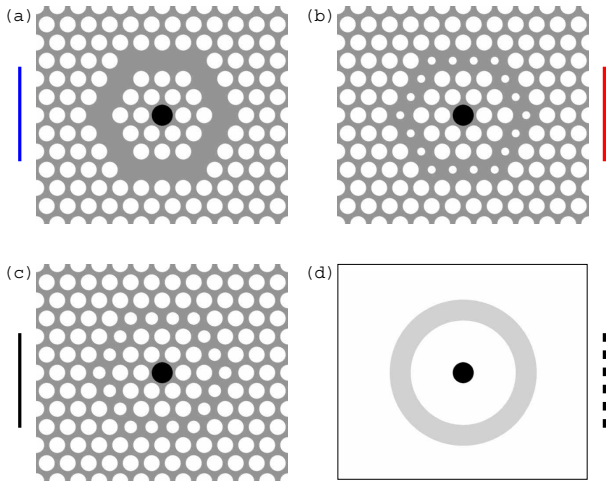

Fig. 1. The studied geometries: microstructure fibers (a)-(c) and the dual-core fiber (d). The refractive index of the core (black) is varied in each geometry. In (a)-(c) the material of the fiber (grey) is silica and the refractive index is 1.444. The cladding is formed by air holes (white). One ring of air holes is used as a defect layer. In (a) the ring of air holes is removed. In (b) and (c) the radius of the holes is reduced to $r = 0.19P$ and $r = 0.3P$, respectively. In the dual core geometry (d) white represents refractive index 1.2114 (the average index of the cladding of the microstucture fiber), black is the core, and grey is the outer core. Three values for the outer core refractive index are considered: 1.444, 1.3859, and 1.299. They correspond to the average values of the defect rings of the microstructure fibers in (a)-(c), respectively. The color coding of the different geometries used in Fig. 4 is shown next to the figures. Dual core fibers are represented by dashed curves with the same colors than the corresponding microstructure fibers.

of the wavelength λ. The effective index is $n_{\text{eff}} = \beta/k_0$, where β is the wavevector and k_0 is the free space wavevector. The dispersion parameter D is numerically calculated as

$$D = -\frac{\lambda}{c}\frac{\mathrm{d}^2 n_{\text{eff}}}{\mathrm{d}\lambda^2}, \tag{1}$$

where c is the velocity of light in free space. The value of the largest negative dispersion is targeted for the operating wavelength $\lambda = 1.55\mu$m, which fixes the period of the cladding. We do not include material dispersion in the simulations as the considered geometric dispersion values are so high that the effect of material dispersion is vanishingly small.

The effective area of a mode A_{eff} is calculated as [21]

$$A_{\text{eff}} = \frac{[\int I(r)\mathrm{d}r]^2}{\int I^2(r)\mathrm{d}r}, \tag{2}$$

where I is the intensity of light and the integrals are over the cross section of the fiber. In all calculations, the simulated cross-sectional area of the fiber was $12P \times 12P$ and each period P was divided in 48 computational grid points.

4. Optimization for large negative dispersion

Typical examples of effective index and dispersion parameter curves as functions of the wavelength for the considered geometries are shown in Fig. 2. The effective index of the third lowest

#5959 - $15.00 US Received 2 December 2004; revised 13 December 2004; accepted 18 January 2005

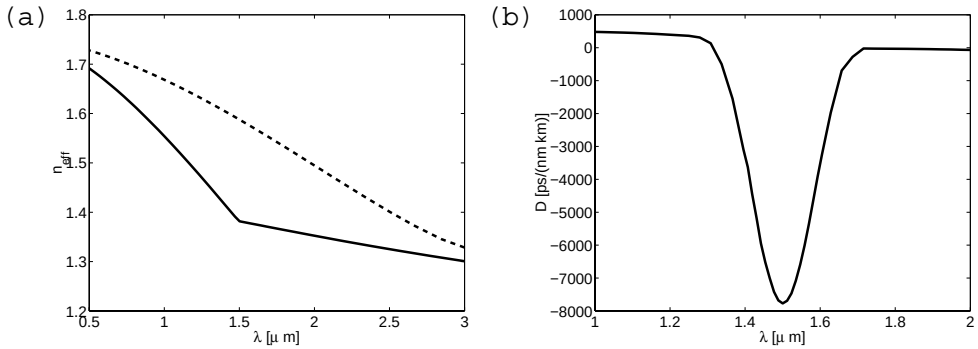

Fig. 2. (a) Effective index of three lowest energy fiber modes. Two lowest energy modes are degenerate (dashed curve). (b) Dispersion parameter calculated from the third mode [solid curve in (a)]. Geometry of the fiber is depicted in Fig. 1(a). The refractive index of the fiber core is $n_{core} = 1.753$ and the period of the cladding lattice is $P = 1.163$ μm.

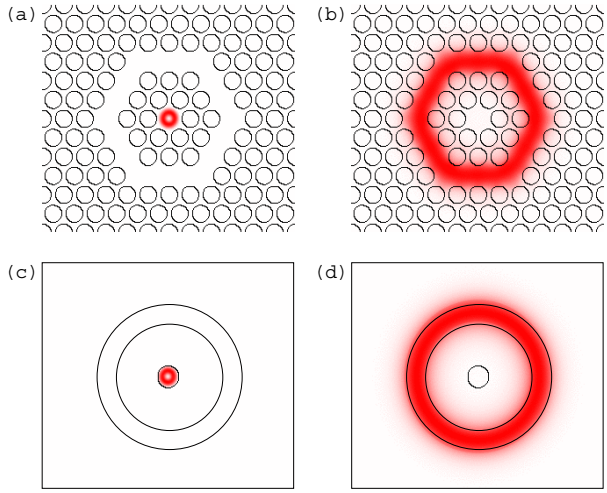

Fig. 3. At short wavelengths the eigenmodes of the microstructure fiber (a) and the dual-core fiber (c) are confined to the fiber core and at long wavelengths to the cladding defect (b) and outer core (d), respectively.

energy mode exhibits a kink. The second derivative of the effective index of this mode, and thus the dispersion [Eq. (1)], is large at this point [see Fig. 2(b)]. The mode distribution of this mode is shown in Figs. 3(a) and (b). At short wavelengths, the mode is confined to the core and, at long wavelengths, to the defect ring in the cladding. At the wavelength at which the effective index exhibits a kink the mode suddenly changes from one mode distribution to the other. This is due to an anticrossing of the two individual core-guided and defect-guided modes. These two mode distributions have very different effective indices. Thus at the wavelength at which the mode distribution suddenly changes from the core to the defect, the effective index exhibits the kink [Fig. 2(a)]. The studied dual-core fibers behave similarly [see Figs. 3(c) and (d)]. The same principle of operation has previously been used for the dispersion compensating dual-core fibers [8, 9, 11] and Bragg fibers [15].

The effective index curve follows the effective index of the core at the short wavelength side of the kink and the effective index of the defect at the long wavelength side. Thus the magnitude

#5959 - $15.00 US Received 2 December 2004; revised 13 December 2004; accepted 18 January 2005

of the dispersion can be tuned by changing the relative slopes of the effective index curves of the core and defect modes. The difference in the effective indices of the two mode distributions can be increased by increasing the refractive index of the core n_{core} or decreasing the effective index of the defect mode. Thus we consider core refractive indices $n_{core} = 1.5 \ldots 2.8$ and the different geometries of the defect ring/outer core introduced in Fig. 1.

The values of the dispersion parameter as a function of the core index for the six geometries are shown in Fig. 4(a). The modes of the geometry of Fig. 1(b) and the corresponding dual-core geometry become unguided for $n_{core} > 2.6$ and Fig. 1(c) for $n_{core} > 2$. It can be seen from Fig. 4(a) that the negative dispersion increases strongly as a function of the core index n_{core}. The largest dispersion found for a microstructure fiber is $D = -55000$ ps/(nm km) for $n_{core} = 2.8$ and geometry of Fig. 1(a). The largest dispersion for the corresponding dual-core geometry is $D = -59000$ ps/(nm km).

The influence of the different geometries to the dispersion depends on n_{core}. For small n_{core}, the geometries that have smaller index in the defect/outer core have larger negative dispersion as expected. However, for large n_{core} the situation is reversed and the geometries with higher index in the defect ring/outer core have larger dispersion. Also, for small n_{core} the negative dispersion of the microstucture fiber is either slightly larger than that of the corresponding dual-core geometry or they are practically equal. For large values of n_{core} the dual-core fibers have larger dispersion than the corresponding microstructure fibers.

The mode distributions at the wavelength of large dispersion are of the form shown in Fig. 3(b) and (d) and thus different from the Gaussian-like mode distributions of the standard single mode fibers. However, in principle the coupling is possible since the mode field diameters of single mode fibers are larger or of same order of magnitude than the diameters of the defect ring/outer core of the considered geometries. Thus there is a substantial overlap of the modes. Also, the refractive index of the core is large and thus the coupling to the core is low. This issue is a topic of a further study. Coupler from a Gaussian beam to an annular mode of a Bragg fiber has been studied in Ref. [22]. There also exist a wide variety of mode converters that are based on having a spatial periodicity that matches the intermodal beat length of the modes in question [23].

The large dispersion found in the fiber is due to the use of the third mode. The mode distribution of the third mode changes abruptly from being confined in the core to be confined in the defect ring in the cladding as a function of the wavelength. The first and second modes, which are degenerate, do not exhibit this behavior, instead their mode distribution is confined close to the core and retains gaussian-like shape. Thus, in this case, to get the high values of dispersion, the use of a multimode fiber is necessary. Care has to be taken in order not to couple light in the other modes. The propagation constants and mode distributions of the different modes are very different and thus coupling between the modes induced by microbending or fabrication inaccuracies of the fiber is unlikely. Moreover, the dispersion values of the fiber are so high that only short lengths of fiber are needed in order to achieve dispersion compensation, which also reduces coupling between modes.

5. Optimization for large mode area

Usually a geometry which exhibits large dispersion has a small mode area. The effective mode areas A_{eff} of the studied geometries, calculated according to Eq. (2), are shown in Fig. 4(b). If each geometry is studied separately, it can be seen that the effective area decreases as the dispersion increases. However, the effective areas of the geometry in Fig. 1(c) and the corresponding dual-core geometry do not decrease as fast as for the other geometries. Thus it is advantageous to use that geometry in order to optimize the effective area and still achieve a large dispersion. The largest dispersion values for these geometries ($n_{core} = 2$) are -19000 ps/(nm km) and

#5959 - $15.00 US Received 2 December 2004; revised 13 December 2004; accepted 18 January 2005

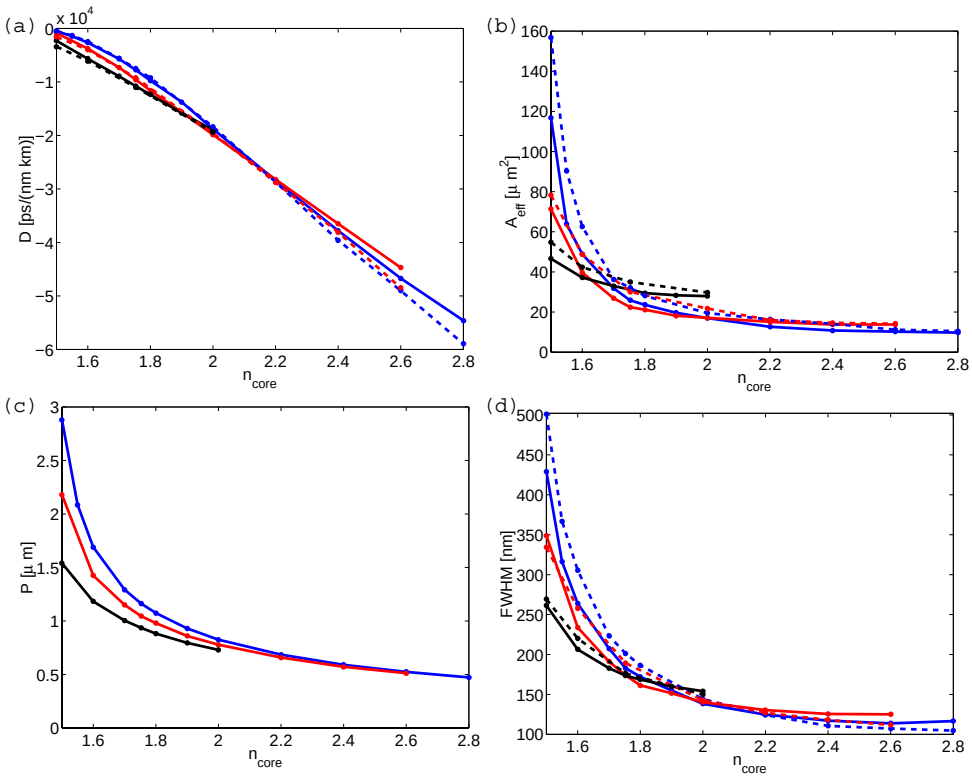

Fig. 4. (a) Largest value of the negative dispersion parameter D for the different geometries as a function of the refractive index of the core n_{core}. (b) The effective areas A_{eff} of the eigenmodes at the wavelength $\lambda = 1.55\mu$m at which the mode changes from the inner core to the outer core. (c) Periods P of the microstructure fibers. The value of the period is adjusted so as to get the largest negative dispersion for the wavelength $\lambda = 1.55\mu$m. (d) The full width at half maximum (FWHM) of the negative dispersion. The color coding of the curves is explained in Fig. 1. Solid blue curve represents the geometry of Fig. 1(a), red curve represents (b), and black curve (c). The dashed curves represent dual-core geometries: blue dashed curve has outer core index 1.444, red 1.3859, and black 1.299. Thus the colors indicate the microstructure geometry and the corresponding average dual-core geometry.

#5959 - $15.00 US Received 2 December 2004; revised 13 December 2004; accepted 18 January 2005

-19400 ps/(nm km) for microstructure and dual-core fibers, respectively. The mode areas of these geometries are 30 μm^2. This feature is not reflected in period size of the microstructure fiber cladding, which is illustrated in Fig. 4(c). It can be stated that the effective mode areas cannot straightforwardly be deduced from the size of the period.

Effective mode area $A_{\text{eff}} = 80$ μm^2 comparable to that of the standard single mode fiber has dispersion -1600 ps/(nm km). It is achieved for a dual-core geometry with $n_{core} = 1.5$ and outer core index 1.3859. The absolute value of the dispersion can be increased if smaller mode areas are allowed. For example dispersion the geometry with $D = -2500$ ps/(nm km) has $A_{\text{eff}} = 60$ μm^2. It is a dual-core geometry with $n_{core} = 1.6$ and outer core index 1.444. The effective mode areas of the large dispersion geometries [$D = 55000$ ps/(nm km) and $D = -59000$ ps/(nm km)] considered in the previous section are both 10 μm^2, which is also reasonably large. Note that the effective mode areas here correspond to the defect ring/outer core mode distributions that are of the form shown in Figs. 3(b) and (d).

6. Full width at half maximum (FWHM) of the negative dispersion

The values of the full widths at half maximum of the dispersion curves [such as in Fig. 2(b)] are shown in Fig. 4(d). It can be seen that the FWHM decreases as the negative dispersion increases [compare to Fig. 4(a)]. However, the smallest FWHM, corresponding to the largest dispersion $D = -59000$ ps/(nm km), is still 105 nm. For the large mode area geometry with mode area $A_{\text{eff}} = 80$ μm^2 (dual-core fiber, $n_{core} = 1.5$, outer core index 1.3859), the FWHM is as large as 330 nm. Note that the FWHM gives only an order of magnitude estimate of the range where dispersion compensation can be realized: the actual range is narrower. Note also that in this paper we did not consider dispersion slope compensation, which could be included in further optimization of the geometries.

7. Conclusions

We have studied and optimized dispersion compensating fiber geometries. We considered different microstructure fiber geometries, with three types of defect rings in the cladding, and corresponding average-index dual-core geometries. The core refractive index of the geometries was varied in the range $1.5 \ldots 2.8$. The largest negative dispersion achieved was $D = -55000$ ps/(nm km) for a microstructure fiber and $D = -59000$ ps/(nm km) for a dual-core fiber. We have also studied the trade off between the mode area and dispersion. A geometry which has an effective mode area $A_{\text{eff}} = 80$ μm^2 comparable to that of the standard single mode fiber has dispersion -1600 ps/(nm km). The geometry with the best trade-off of mode area and dispersion has -19400 ps/(nm km) and $A_{\text{eff}} = 30$ μm^2. The full widths at half maximum of the dispersion of all the studied geometries were larger than 100 nm which is enough to cover both the C and the L bands of the Erbium doped fiber amplifier.

The mode areas calculated in this paper are larger than the ones predicted previously, especially for the microstructure fiber. This is because the considered geometry offers an additional degree of freedom since, apart from the core and cladding refractive indices, one can also vary the defect ring refractive index. The mode area depends mostly on the defect ring index: when the difference of the indeces of the defect ring and the cladding is small, the mode can spread slightly outside the defect ring.

The dispersion values achieved in this paper are extremely high as compared to the previous studies with similar fiber geometries. One reason for this is that we have used very high refractive indices in the inner core, which makes the refractive index difference between the core and defect ring/outer core large and thus increases the dispersion. Usually high refrective index of the core is not preferred since the coupling from a standard optical fiber is difficult. In the studied geometries the high refractive index of the core is not an obstacle, because the mode

#5959 - $15.00 US Received 2 December 2004; revised 13 December 2004; accepted 18 January 2005

residing mainly in the defect ring/outer core is utilized.

Acknowledgments

We thank Emil Aaltonen foundation and the Academy of Finland for support (Project Nos. 53903, 205454).

#5959 - $15.00 US Received 2 December 2004; revised 13 December 2004; accepted 18 January 2005